Acta Materialia 286 (2025) 120702

Contents lists available at ScienceDirect

Acta Materialia

journal homepage: www.elsevier.com/locate/actamat

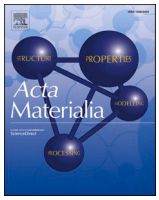

Kinetics of ferroelastic domain switching with and without back-switching events: A phase-field study

Avisor Bhattacharya , Mohsen Asle Zaeem *

Department of Mechanical Engineering, Colorado School of Mines, Golden, Colordao 80401, United States

ARTICLE INFO

Keywords:
Ferroelasticity
Kinetics
Switching
Back-switching
Phase-field modeling

ABSTRACT

Incomplete domain switching in ferroic materials under external stimuli occurs frequently and it significantly affects their performance. In this study, we perform phase-field simulations of ferroelastic domain switching in yttria-stabilized zirconia to investigate the kinetics of domain switching. For a wide range of applied loads, the kinetics of domain switching follows the Kolmogorov-Avrami-Ishibashi (KAI) model. The domain wall velocity remains constant under a constant load but accelerates when the load is gradually increased over time. The steady movement of domain wall is observed to dominate the kinetics of ferroelastic domain switching. The present study reveals that during switching, some degree of back-switching simultaneously may occur depending upon the applied load and microstructures. Also, sharp corners on domain walls intensify the switching activity, and they often promote back-switching during loading, leading to incomplete domain switching. Increase in back-switching is subsequently followed by another re-switching event that ultimately results in a large deviation from KAI model and a greater absorption of applied deformation.

1. Introduction

Over the past few decades, a significant amount of experimental and theoretical work has been devoted to understanding the complex mechanisms of domain switching in ferroic materials [1]. The fact that domain switching brings about intriguing material properties has catapulted ferroic materials into critical applications like non-volatile memory devices [2], actuators [3], thermal-bearing-coating [4], and many more. On cooling below a critical temperature, an unstable phase transforms into a ferroic phase with a crystal structure of lower symmetry, leading to different crystallographically equivalent degenerate variants that constitute domains in the microstructure. Under external stimuli such as magnetic, electric, or stress fields (or a combination of these), one or more domains switch into other domains that have lower free energy in the energy landscape in ferromagnetic, ferroelectric, or ferroelastic materials, respectively [1,5]. The mechanism of domain switching is still not completely understood particularly in ferroelastic materials even though a significant amount of works has contemplated in ferroelectric behavior mediated by ferroelasticity.

Domain switching is a first order phase transition which involves nucleation followed by growth [1]. Several experimental and theoretical works have demonstrated that nucleation takes place on various two-dimensional defects such as domain walls [6,7], grain boundaries [8,9], phases interfaces [10,11], and free surfaces [12], similar to the usual phase transformation in metals and alloys. Subsequently, domain walls migrate as favorable domains engulf the other domains. At the atomic scale, the movement of domain walls involve jumping of atoms or ions and this jump is orchestrated by either thermal activation or by other external stimulus resulting in time-dependent polarization or deformation 'creep' behavior [13]. Based on this consideration, some researchers have proposed that the velocity of domain walls (v) is proportional to $\exp(-U/kT)$, where U is the barrier height related to the external stimulus [14], T is the temperature, and k is the Boltzmann constant. Some previous works suggested that the competition between domain wall pinning and elastic energy should actually result in a more complicated relation like $v \propto \exp\left[-\left(\frac{U}{kT}\right)\left(\frac{f_c}{f}\right)^{\mu}\right]$, where f_c is the critical pinning force at $T = 0$ and $\mu = 1$ [15,16]. On the other hand, the thermodynamics of interface-controlled growth applied to domain switching suggests that switching rate should be directly proportional to the stimulus [17,18]. In $LiTaO_3$, domains were indeed observed to move with a steady velocity as suggested by the theory of diffusionless growth [19]. In an intriguing observation, it was found in $Pb(Zr,Ti)O_3$ (PZT) thin film that the domain wall movement in one dimension can be

* Corresponding author.
E-mail address: zaeem@mines.edu (M. Asle Zaeem).

https://doi.org/10.1016/j.actamat.2024.120702
Received 22 July 2024; Received in revised form 11 December 2024; Accepted 30 December 2024
Available online 31 December 2024

explained by diffusional parabolic growth [20]. There are some instances where the domain walls have been observed to have 'jerky' motion [21–23]. The velocity of domain wall in ferroelectric materials has been observed to be decreasing with time either due to defect pinning, opposing field or interaction with the other domain walls, but it is eventually activated by the applied field which results in 'jerky' motion [22,24,25]. This means that in the absence of these obstructions, the domain walls should accelerate. In $CaTiO_3$, it was shown that in absence of lattice pinning, the domain walls indeed accelerate [26]. Although, the entities opposing domain wall motions are well identified in ferroelectric materials, the behavior of domain walls is not completely understood in purely ferroelastic materials.

The study of kinetics of domains switching is essential for any application pertaining to ferroic behavior. Several attempts have been made to understand the kinetics of domains switching theoretically or experimentally. The Fokker-Planck equation has been used to study the kinetics of domains switching; in this model, a fluctuation term is considered for the initial nucleation stage, a hydrodynamic term controls the subsequent growth of a distribution of switching nuclei, and the Ostwald ripening is applied to describe the growth of favorable domains [17,27,28]. However, this model does not consider the change in kinetics due to impingement of growing domains. In a pioneering work, the Avrami-Kolmogorov approach was adopted by Ishibashi who proposed a model for kinetics of domain switching (henceforth noted as 'KAI' model) [29,30]. The KAI model considers two possibilities regarding the nucleation step: in the first case (category 1) a finite and constant nucleation rate precedes the growth, and in the second case (category 2), the nucleation of new domains quickly ceases according to this equation:

$$V = 1 - exp\left(-\frac{t}{t_0}\right)^n \tag{1}$$

where V is the volume fraction of a domain that is switching in time t, and the time exponent n depends on the dimensionality and the category of nucleation. Good performance of this model was observed by experiments [22,31]. A study on epitaxial $BiFeO_3$ thin film revealed that for a high applied electric field, KAI model satisfactorily describes the switching kinetics, but for a low applied electric field, the exponent n is less than unity which is impossible in KAI model [32,33]. A modified approach was adopted later [29,33], where nucleation plays the dominant role in switching and this is known as 'nucleation limited switching' (NLS). In polycrystalline materials, the dominant nucleation favors NLS over KAI theory as domains are pinned by grain boundaries. However, it was pointed out that in polycrystalline materials, a modified KAI model is needed to consider the coherence length of nucleation spanning over several grains [9]. Apart from NLS model, other non-KAI models have been proposed to explain the kinetics of domain switching [24,34]. Most of the studies on kinetics of domain switching have been performed in ferroelectric materials where the size of capacitor under applied electric field can also influence the complex nucleation and propagation of domain walls [24,35,36]. The kinetics of domain switching in purely ferroelastic materials has not been explored yet.

Very often, the domain switching does not go to completion. For instance, in PZT film deposited on $SrRuO_3$ substrate, despite applying high voltage, one of the variants does not completely disappear [37]. It was also observed that despite application of electric field to attain a uniform polarized state, some opposite polarized states also remain in the same material [35]. In both cases, domain walls moved back recovering the original domain configurations before switching when the external electric field was withdrawn. This phenomenon is known as 'back-switching', which has grabbed the attention of research community particularly in ferroelectric materials because of its deleterious effects on non-volatile memory application resulting in loss of polarization retention and loss of data [38,39]. The mechanism of back-switching has not been completely understood yet. Some researchers have proposed that the depolarizing field, arising out of imbalance between polarization charge and that formed at the electrode, results in back-switching [40–42]. On the other hand, others, like Gruverman [43], have proposed that in metal-oxide-semiconductors, internal bias in depletion zone drives the back-switching. It was demonstrated that the back-switching originates from grain boundaries by nucleation at the defect sites followed by propagation of domain walls similar to switching [44]. This theory, however, cannot explain the back-switching behavior in single crystals. Morelli has shown that in single crystals, the domain walls develop steps, and it was theorized that these steps play a role in back-switching even though the exact mechanism of back-switching was not revealed [45]. On the other hand, if the oppositely polarized/strain state already exists in the microstructure, then the back switching can easily take place by relaxation of high energy domain wall [35]. The latter mechanism appears to be energetically more favorable as it does not require the nucleation step. But, due to lack of understanding of the mechanism of formation of back-switched regions during loading, there still exists a gap in understanding this phenomenon.

In the present work, we intend to study the kinetics of purely ferroelastic domain switching by using a phase-field model. Phase-field model has become a reliable and very powerful tool to study the evolution of microstructure. Recent advances in phase-field modelling techniques for solid state phase transformations have allowed to study the evolution of microstructures under the application of stress [46–48], electric [49–51] and magnetic fields [52–54]. Particularly, phase-field simulations of ferroelectric materials have enhanced insight into the mechanism of domain switching required for critical applications. In these models, free energy functional considers polynomial function of polarizations in accordance with Landau theory [49]. However, the model considers that the gradient in polarization contributes to domain wall energy and coherent twin boundary energy is neglected. Furthermore, the model apparently overlooks the aspect of conservation of domains during switching [55]. In comparison to ferroelectric behavior, phase-field simulation of purely ferroelastic domain switching driven by external stress field, is rather scarce. Pi adopted a multiphase field framework to simulate the domain switching under arbitrary constant load [56]. Sun has attempted to investigate the impact of ferroeleastic domain switching on toughness of yttria-stabilized-zirconia (YSZ), but the model is capable to switch between only two domains [57]. Zhou has adopted an improvised model with three variants satisfying conservation and simulated the evolution of variants during ferroelastic deformation in YSZ film [58]. However, the major limitation of this model is that it cannot be applied to ferroelastic switching involving more than three variants. None of these works have attempted to study kinetics of ferroelastic domain switching which is still elusive to date.

In this work, we employ our recently developed ferroelastic domain switching model [59] for arbitrary number of crystallographic variants ensuring the conservation of the domains. One major advantage of using this phase-field model is that it automatically takes care of overlapping of growing domains without defining any specific criteria for impingement of domains. Also, the domain switching in the present model is strongly influenced by the energy of twin boundaries. In this study, we have chosen the tetragonal-prime (t') phase in yttria-stabilized zirconia (YSZ) which is well known to be a purely ferroelastic material [60,61]. Using phase-field simulations under various loading conditions and microstructures, we have demonstrated the formation of back-switching regions during loading and uncovered the underlying mechanism driving this behavior. This phenomenon has a significant impact on the properties of certain ferroic materials.

2. Computational methodology

2.1. Phase-field model

Let us consider N number of crystallographic variants which are

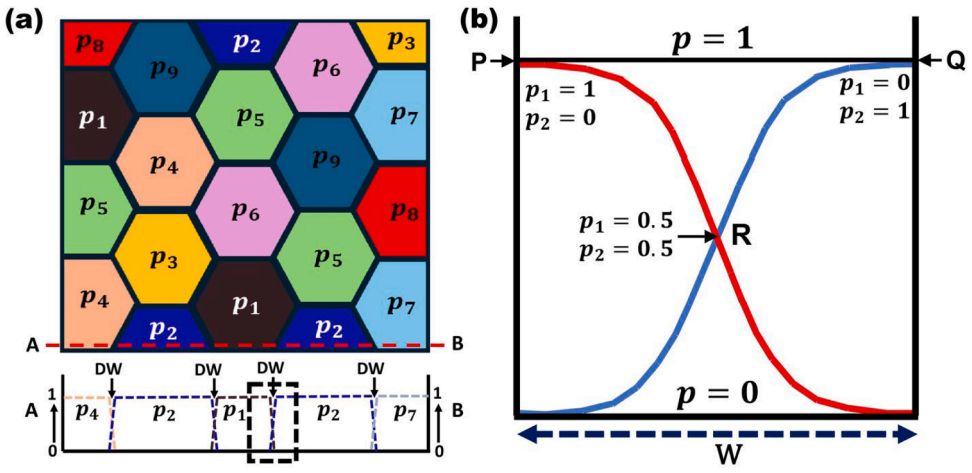

Fig. 1. (a) The schematic of domains with hypothetical 9 crystallographic variants denoted by 9 phase field variables. Along the intersecting line AB, the phase-field profiles are shown below. The domain wall (DW) between p_1 and p_2 in (a) is magnified in (b). It is evident that the summation of the phase field variables p_1 and p_2 is unity in every region of the domain.

represented by phase-field variables $p_1, p_2, p_3 \ldots p_N$. Each phase-field variable takes the value of unity in the corresponding crystallographic variant, and it smoothly varies from 1 to 0 in the domain wall; the schematic in Fig. 1 shows how two phase-field variables vary between two neighboring domains and the domain wall between them. The total free energy $F\left(p_i, \nabla p_i, \varepsilon_{pq}^{el}\right)$ of the entire volume consisting of domains separated by domain walls have three components: the free energy of the bulk domains $f_{bulk}(p_i)$, the domain wall energy due to the gradient of the phase-field variables $f_{grad}(p_i)$, and the free energy due elastic deformation $f_{elast}(\varepsilon_{pq}^{el})$:

$$F(p_i, \nabla p_i, \varepsilon_{pq}) = \int \left[f_{bulk}(p_i) + f_{grad}(\nabla p_i) + f_{elast}(\varepsilon_{pq})\right] dv \tag{2}$$

The following form of bulk free energy function is considered:

$$f_{bulk} = A\left(\sum_{i=1}^{N} p_i - 1\right)^2 + B\sum_{i\neq j}^{N} p_i^2 p_j^2 + C_1 \sum_{i\neq j\neq k}^{N} p_i p_j p_k + C_2 \sum_{i\neq j\neq k\neq l}^{N} p_i p_j p_k p_l + \ldots\ldots + C_{N-2} p_i p_j p_k p_l p_m \ldots p_N \tag{3}$$

During domain switching, the total volume of the crystallographic variants remains conserved due to identical density of the variants. The conservation of the domains is implemented by setting a high value for the coefficient A which penalizes the free energy if $\sum_{i=1}^{N} p_i \neq 1$. The second term is multiwell potential function where coefficient B represents the barrier height. The terms with coefficients $C_{1,2,3..n-2}$ are multiobstacle potential functions and they consider all possible interactions of the domains [59]. The free energy due to gradient of p_i in domain wall is given by

$$f_{grad} = \sum_{i=1}^{N} \frac{k_p^2}{2} |\nabla p_i|^2 \tag{4}$$

where k_p is the gradient energy coefficient. Finally, the elastic energy has the following form:

$$f_{elast} = \frac{1}{2} \varepsilon_{pq}^{el} E_{pqrs} \varepsilon_{rs}^{el} \tag{5}$$

where ε_{pq}^{el} is the elastic strain tensor and E_{pqrs} is the fourth order elasticity modulus tensor. The phenomenological minimization of $F(p_i, \nabla p_i, \varepsilon_{kl})$ results in the evolution of each phase field variable as given below:

$$\frac{\partial p_i}{\partial t} = -M_p \frac{\delta F}{\delta p_i} = M_p \left[\nabla . \frac{\partial F}{\partial \nabla p_i} - \frac{\partial F}{\partial p_i}\right] = M_p \left[k_p^2 \nabla^2 p_i - 2A\left(\sum_{i=1}^{N} p_i - 1\right) - 2B\sum_{i\neq j} p_i p_j^2 - C_1 p_{j\neq i} p_{k\neq i} - C_2 \sum_{i\neq j\neq k\neq l}^{N} p_j p_k p_l \ldots\ldots\ldots - C_{n-2} p_j p_k p_l p_m \ldots . p_N - \frac{\partial f_{elast}}{\partial p_i}\right] \tag{6}$$

where M_p is phase-field mobility. The total strain (ε_{pq}^{tot}) is the sum of elastic strain (ε_{pq}^{el}) and stress-free strain tensor $(\varepsilon_{pq}^{*,i}$ where,$i = 1, 2, ..N)$ for all the N variants. The total strain is also the sum of homogeneous strain ε_{pq}^{hom} and heterogeneous strain $\delta\varepsilon_{pq}$. The stress-free strain tensors are interpolated in the entire volume by interpolation function $h(p) = 3p^2 - 2p^3$ such that $h(0) = 0$ and $h(1) = 1$ and $h(p)$ smoothly varies with p. Therefore, the elastic strain tensor is given as follows:

$$\varepsilon_{pq}^{el} = \varepsilon_{pq}^{tot} - \varepsilon_{pq}^{*} = \varepsilon_{pq}^{hom} + \delta\varepsilon_{pq} - \sum_{i=1}^{N} \varepsilon_{pq}^{*,i} h(p_i) \tag{7}$$

We assume linear elasticity so that the second order stress tensor $\sigma_{pq} = E_{pqrs}\varepsilon_{rs}^{el}$. We also assume that elasticity moduli are the same for all the variants and thus,

$$\frac{\partial f_{elast}}{\partial p_i} = -\frac{1}{2} h'(p_i) \left[\varepsilon_{pq}^{*,i} E_{pqrs} \varepsilon_{rs}^{el} + \varepsilon_{pq}^{el} E_{pqrs} \varepsilon_{rs}^{*,i}\right] \tag{8}$$

Finally, we assume that loading rate is slow enough that the mechanical equilibrium prevails and thus:

$$\frac{\partial \sigma_{pq}}{\partial x_q} = 0 \tag{9}$$

The t' phase in YSZ has three tetragonal variants which are represented by three phase-field variables p_1, p_2 and p_3 [62]. The c axes of the tetragonal unit cells of the three variants lie along pseudocubic [100], [010] and [001] directions. Since the ferroelastic domain switching in YSZ is exploited in thin thermal-barrier-coating, the plane stress condition prevails in the present model. It should be noted that the polarization of thin film of ferroelectric material can also be subjected to

similar two-dimensional plane stress condition. The details of the model equations of ferroelastic domain switching in YSZ are discussed in our recent work [59].

2.2. Numerical implementation

All the governing equations are solved by using finite difference methods. The Laplacian operator is approximated by a second order scheme and first order explicit scheme is applied for time stepping. Mechanical equilibrium in Eq. (9) is solved iteratively until the difference of displacements at every point in consecutive iterations are less than $10^{-5}\Delta x$. In the present work, the phase-field variables p_1 and p_2 represent in-plane a_1 and a_2 domains in which c axis of the unit cell is aligned along x_1 (crystallographic [100]) and x_2 (crystallographic [010]) axes, respectively, while in c domain, c axis lies along x_3 (crystallographic [001]) (as shown in inset figures in Fig. 2a). We have applied load along x_2 on the top side of the square simulation domain where the displacement is either maintained to a specific value (constant load) or it is varied with time (varied loading condition, see the inset figures in Fig. 2a). In one set of simulations, we have applied constant loads by maintaining constant displacements in such a way that constant levels of strain of 0.75 %, 0.85 %, 1.2 %, 1.25 % and 2.5 % are achieved. In another set of simulations, load is applied by varying the displacement with time in such a way that the strain rates of 10^{-4} and 10^{-6} s^{-1} are achieved. The bottom side of the simulation domain has zero displacement whereas Nuemann boundary condition is applied on left and right sides of the domain. Nuemann boundary condition is also applied for phase field variables. In the present work, we have used the same meshing and model parameters as adopted in our previous work where we have demonstrated the convergence behavior of the present model [59]. In the present work, we have chosen to study the kinetics of ferroelastic domain switching at 500 °C and the values of the simulation parameters are taken from our previous work where the justification of these parameters were also discussed in detail [59]. It should be noted that the present model precisely captures the ferroelastic deformation and diffusionless mechanism of domain switching at 500 °C accounting for the dependency of the model parameters on temperature. Square simulation domains with dimensions of 720 nm × 720 nm represent two initial microstructures each consisting of c, a_2 and a_1 domains. These microstructures are taken from the experimental observations of YSZ single crystal and are labelled as 'Microstructure 1′ and 'Microstructure 2′ (see the inset figures in Fig. 2a) [63].

Noguchi performed tensile tests on several 170 mm long YSZ specimens having different compositions and the stress-strain curve was reported to deviate from linearity above 600 MPa [64]. However, several samples in that experiment were fractured in the transition region between gauge and grip suggesting that the presence of defects particularly at the stress concentration sites might have resulted in much lower strength. A better estimation of yield strength has been reported by a recent bending test of microcantilever beam specimens [65]. It was observed that the yield strength under tension in YSZ is highly sensitive to the orientation of crystal, and it varies in the range of 2–7 GPa. Following these experiments, we applied displacements resulting in strains of 0.85 %, 1.25 % and 2.5 %, and stresses of 1, 2 and 5.2 GPa in Microstructure 1, respectively, as shown in Fig. 2. Similarly, in Microstructure 2, we have applied strains of 0.75 %, 1.2 % and 2.5 % resulting in stresses of 1.3 2.7, and 6.3 GPa, respectively. In addition, we applied deformation at two strain rates of 10^{-4} and 10^{-6} s^{-1}. These strain rates are often applied to study the deformation behavior in YSZ [61,66,67].

It should be noted that ferroelastic toughening in t'-YSZ is primarily exploited in thin thermal barrier coating (TBC), and several previous studies have adopted 2D simulation domains exploiting the geometry of this application [56,57]. However, some phase-field simulations of thin ferroelectric films deposited on different substrates adopted 3D simulations to capture the effect of mismatch strains, and these studies have revealed the role of mismatch strain on the evolution of domains [12,55,68]. However, the 2D simulation study of domain switching without intervention of any mismatch strain could also unravel the mechanism of ferroelectric domain switching [49,50]. Therefore, we have adopted a 2D numerical domain with plane stress approximation in the present work without considering any mismatch strain. On the other hand, a 3D simulation of thin film of $PbTiO_3$ which has exactly the same three tetragonal domains as YSZ, has revealed that despite the influence of mismatch strain caused by the substrate, the domain walls run nearly parallel to thickness of the thin film [55]. This suggests that microstructure of any 2D cross section parallel to the interface between film and substrate is practically identical.

Experimental and numerical simulation in TBC reveal that the topcoat of YSZ after deposition on bond coat develops in plane compressive residual stress of around 300 MPa at the junction of bond coat and topcoat, while for higher thickness of the topcoat, the top surface often develops in plane tensile stress of around 50 MPa [69]. Therefore, even if the microstructure remains the same along the thickness, the residual stress varies significantly. In order to assess the difference in kinetics of the domain switching in YSZ topcoat in actual 3D geometry from the present 2D simulations, we have performed 2D

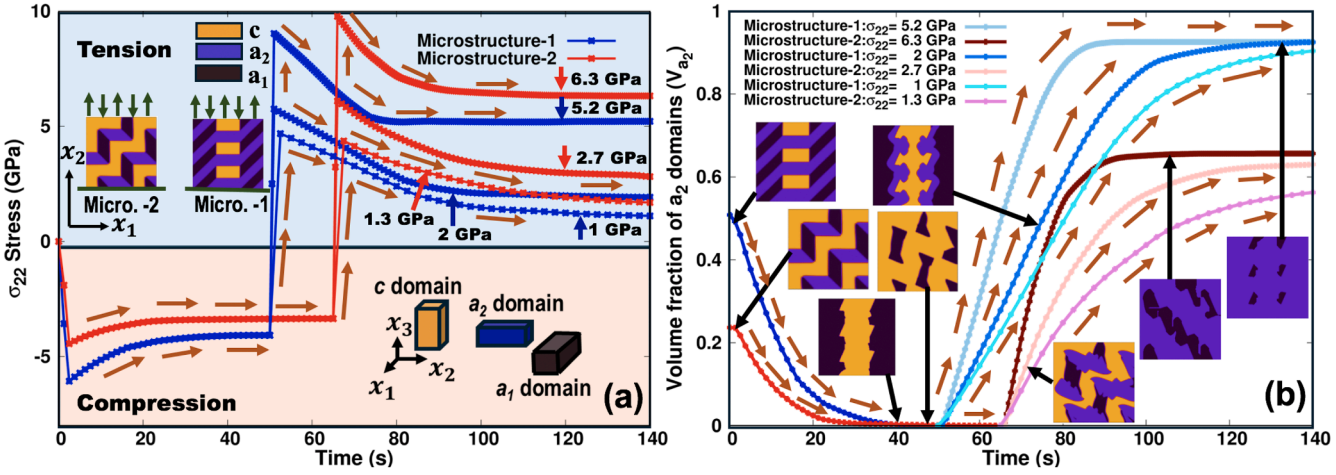

Fig. 2. (a) The variation of σ_{22} with time during 'constant loading' in Microstructure-1(Micro. −1) and Microstructure-2 (Micro.−2) which are adopted from experiment [63]. The microstructures consist of c, a_2 and a_1 domains in which the c-axis of the tetragonal unit cell lies along x_3, x_2 an x_1 axis, respectively. The loading paths and the evolution of a_2 domains in these loading paths are represented by brick red arrows. (b) Due to application of compressive followed by tensile loading along the x_2 axis, a_2 domains gradually diminish in both microstructures under compression and then it reappears under tension.

simulations in Microstructure 1 under strain rate of $10^{-6}\ s^{-1}$ with the addition of homogeneous strains ϵ_{11}^{hom} and ϵ_{22}^{hom} accounting for the residual stress of −300 MPa and 50 MPa. The analysis of the kinetics under the influence of homogeneous strains is presented in section S2 of the supplementary material.

To track the domain wall during switching in regular interval of time, we have located the points representing $p_i = 0.5$, which we identify as the center of a domain wall, along specified direction that contains the locus of center of the domain wall over the entire switching period. We have also calculated the inclination angle (θ) of the domain wall with respect to x_1 axis at the center of the domain wall in every time interval. We have employed a linear interpolation technique to locate $p_i = 0.5$ and locus of this point over regular interval of time allows to calculate the velocity (v) of domain wall. To calculate the inclination of domain wall at a point on it, we fit a cubic polynomial function of the form: $y = a_0 + a_1x + a_2x^2 + a_3x^3$ by using least square method through the (x, y) coordinates of altogether eleven center-points (each determined by interpolation technique) with five points on each side of the given point. The values of θ are then calculated from the derivatives of the fitted cubic polynomial function by using the relation

$$\theta = \arctan\left(a_1 + 2a_2x + 3a_3x^2\right) \tag{10}$$

We have ensured that the fitting of the polynomial function is carried out through the center points of fairly smooth domain wall. From the velocity and the angle of inclination, we have calculated the normal velocity(v_n) of the domain wall along a particular direction by the relation

$$v_n = v/\cos\theta \tag{11}$$

3. Results and discussion

3.1. Compressive and reverse tensile deformation

First, a compressive loading is applied on the microstructures along x_2 direction. In Fig. 2, the applied load and the corresponding evolution of microstructures in response to the loading are shown. The compressive load is applied rapidly and after a very small stress drop, an almost constant level of σ_{22} is eventually attained. Similarly, when subsequently tensile load is applied rapidly, a constant level of σ_{22} is eventually obtained again after an initial stress drop. We treat this type of loading as a 'constant loading' condition where strain due to applied load is approximately constant. Due to compressive stress σ_{22}, a_2 domain switches into c and a_1 domains as its c axis of the unit tetragonal cell is aligned along x_2 direction and compression along x_2 makes a_2 domains unstable [63]. After completion of the compression step, application of tensile load along x_2 results in a higher stability of a_2 domain compared to the other two domains, and therefore c and a_1 domains switch into a_2 domains [59,63,70]. The occurrence of domains under different loading conditions depends on their thermodynamic stability, and therefore, it can be determined by a phase diagram [71]. A tentative phase diagram based on the present work is described in section S3 of the supplementary material. In this phase diagram, we observe the two-phase regions consisting of c and a_1 as well as a_1 and a_2 domains consistent with loads

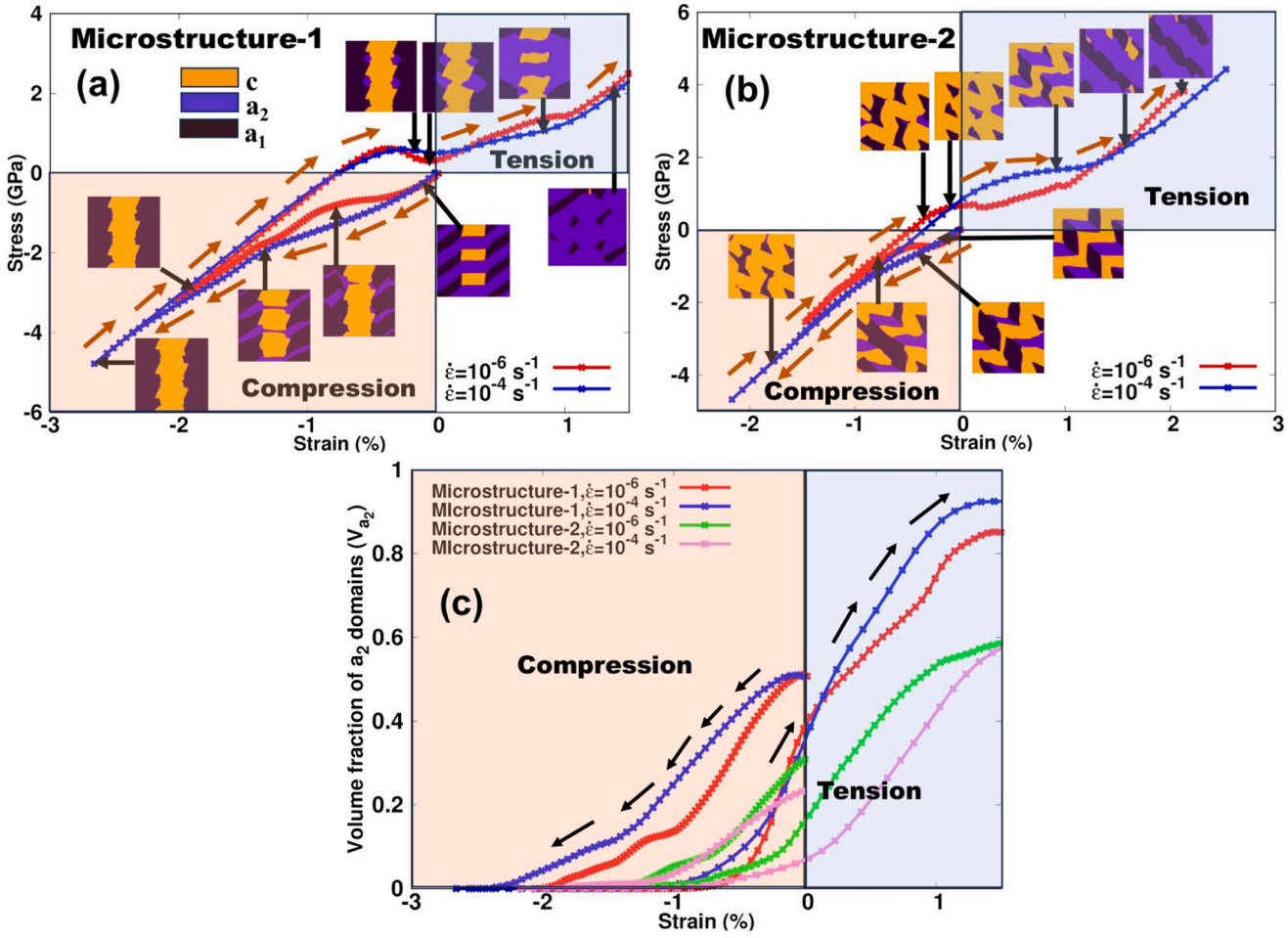

Fig. 3. Evolution of microstructures during compression followed by tension in (a) Microstructure-1, and (b) Microstructure-2 under strain rates of $10^{-6}s^{-1}$ and $10^{-4}s^{-1}$. The loading path is represented by red arrows. The corresponding volume fraction of a_2 domains (V_{a_2}) during loading-reverse loading is shown in (c).

applied. Although complete switching takes by the end of the compression step, in tension, despite the application of a higher level of stress, complete switching is not reached.

In another type of loading, we have applied compression followed by tension with strain rates of $10^{-6}s^{-1}$ and $10^{-4}s^{-1}$, as shown in Fig. 3, which should be considered as 'varied loading' as in this case the applied strain changes with time in response to the applied load. We show that the plots of stress-strain curves under varied loading describe hysteresis curves due to ferroelastic domain switching as shown in Fig. 3a for Microstructure-1 and in Fig. 3b for Microstructure-2. In Fig. 3, during compression, a_2 domains disappear, but they return on tension under varied loading condition in the same way as observed in Fig. 2 under the constant loading. In Fig. 3a and b, we similarly observe that under reverse tensile loading with both the strain rates, switching does not go to completion and the simulations are therefore consistent with the experimental observation [37,70]. In the present work for the first time, we investigate the impact and origin of the incomplete domain switching to close the gap in our understanding of this event.

3.2. The kinetics of domain switching

Incomplete domain switching influences the kinetics of domain switching, and to assess its effect on the overall domain switching behavior, we study the nucleation and growth of a_2 domains during reverse tensile loading in both microstructures under constant and varied loading conditions. Here, we describe the details of kinetics of ferroelastic domain switching in Microstructure-1, and in section S1 of the Supplementary Material, we have included the kinetics and evolution of domains in Microstructure-2. The simulations reveal that the nucleation of a_2 domains take place at $c|a_1$ domain walls which is consistent with the previous experimental observation [6]. As shown in Fig. 4 in Microstructure 1 and Fig. S1 in Microstructure 2, by the application of constant load, the nucleation takes place along the $c|a_1$ domain wall so rapidly that it is very difficult to capture the individual nucleation event. The application of chosen loads uniformly increases the driving force and sharply reduces the critical dimensions of nucleation, and therefore nucleation takes place more rapidly [7]. On the other hand, under the varied loading conditions, the nucleation takes place at specific sites (as shown in Fig. 8 and Fig. S4) after a perceptible incubation time, as indicated in Figs. 3c, 5a and b. In our earlier work, we have shown that the nucleation primarily takes place at corners, crevice and steps on $c|a_1$ domain walls as the nucleation barrier in the range of 10^3kT is easily surmounted in these sites [7]. The nucleation density is estimated to be $1.157 \times 10^{13}\ m^{-2}$ in Microstructure-1 and $1.35 \times 10^{13}\ m^{-2}$ in Microstructure-2 under the varied loading condition. The simulated nucleation density is similar to the experimental measurements, albeit in a nanocapacitor capturing a single nucleation event in a sample having the radius of 35 nm [24]. Such a small study domain however tends to overestimate the nucleation density [24]. In both loading cases, we observe that the nucleation events at domain walls take place almost simultaneously, and they almost simultaneously go to near completion at all the nucleation sites. After nucleation, a_2 domains grow by sidewise motion in our simulations, as predicted by Miller [72].

In Figs. 4b, S1b and 5c, we have plotted $\log[-\log(1-V_{a_2})]$ versus logarithm of time normalized by $t_0 = 1s$ as given by Eq. (1). Through these plots, we have also fitted straight lines. For the constant loading in Figs. 4b and S1b, all the coefficients of determination are above 0.98. From these two figures, we note that the kinetics of domain switching mostly follow the KAI model with time exponent n laying in the range of $1 < n < 2$ (see the KAI model in Eq. (1)). In Fig. S1b, we also observe that switching kinetics in Microstructure-2 for applied load of 2.7 and

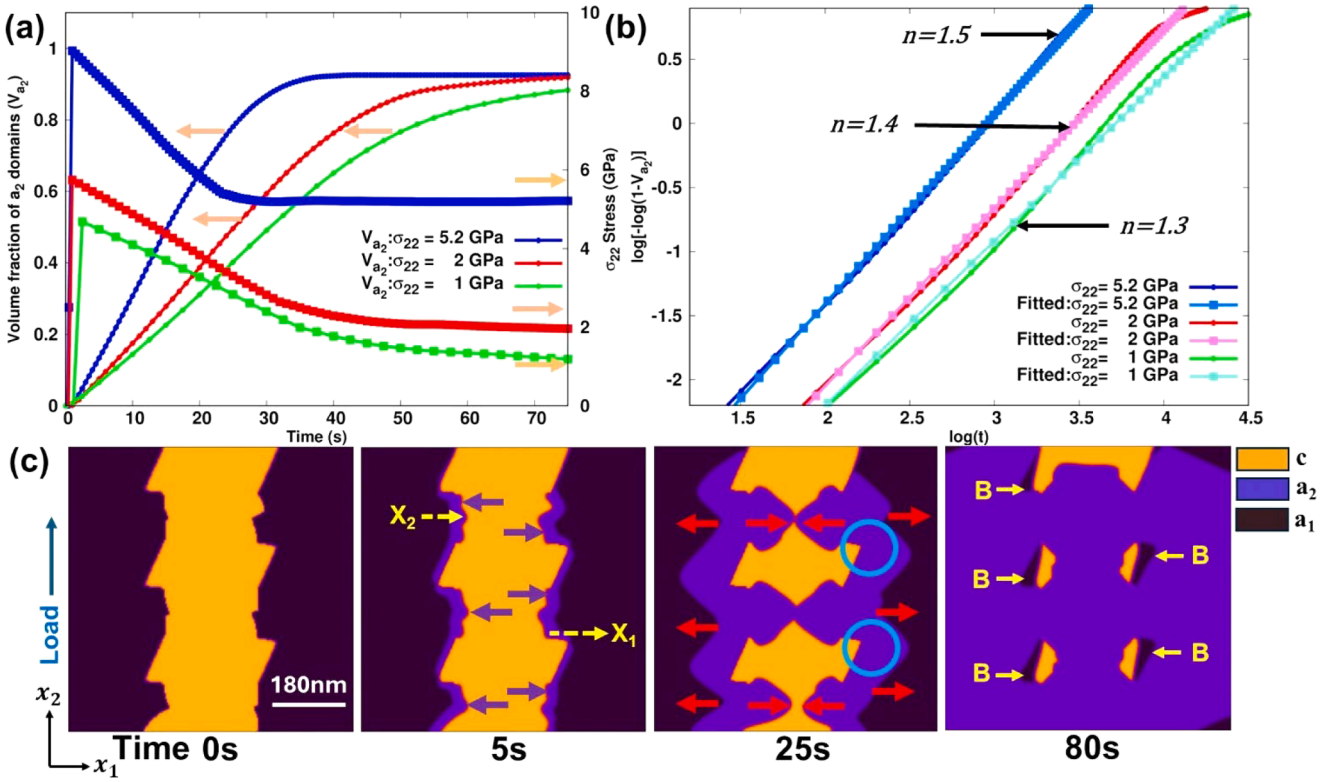

Fig. 4. Nucleation and subsequent growth of a_2 domains at constant tensile loads of 1, 2 and 5.2 GPa in Microstructure-1 obtained after compression as depicted in Fig. 2. (a) In the plots of volume fraction of a_2 domains (V_{a_2}) with time, the square-shaped data points represent the variation of applied stress σ_{22} with time. (b) The plots of $\log[-\log(1-V_{a_2})]$ versus the logarithm of normalized time are approximately linear for different loads. (c) The nucleation and subsequent evolution of a_2 domains for applied stress of 1 GPa. Nucleation sites are marked by blue arrows at 5 s, and red arrows indicate the direction of domain wall propagation at 25 s. Back-switched regions are marked by 'B' at 80 s.

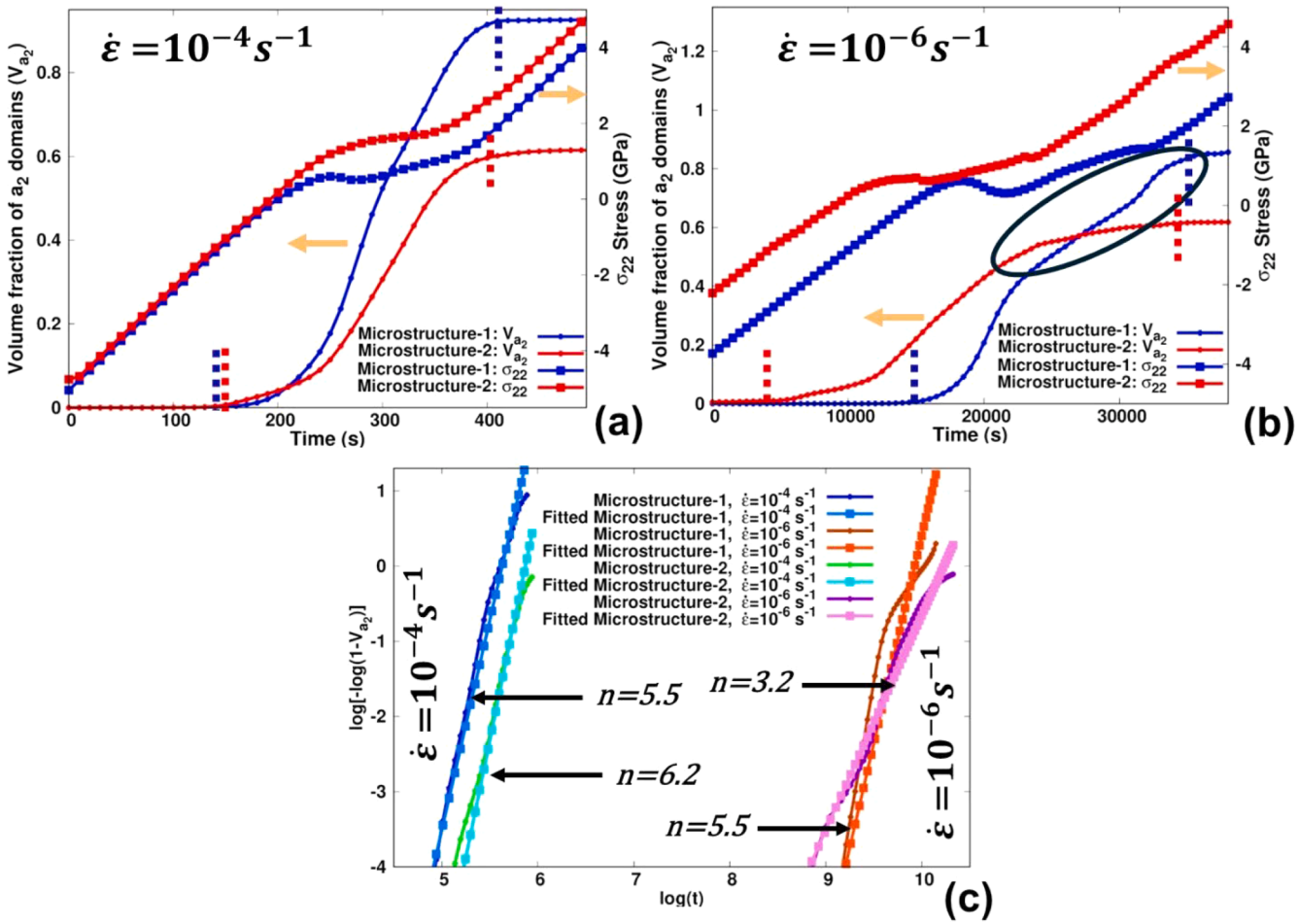

Fig. 5. The variation of volume fraction of a_2 domains in both the microstructures versus time for strain rates of (a) $10^{-4}s^{-1}$ and (b) $10^{-6}s^{-1}$. The non-smooth evolution of a_2 domains are marked by black colored elliptical lines. The dotted lines mark the start and end of the switching. (c) The kinetics of domain switching in the simulations are compared with the KAI model.

1.3 GPa result in $n < 1$; such unrealistic values are attributed to non-stabilization of the kinetics to a final constant and the time-independent volume fraction of a_2 domains which is not consistent with the assumptions of KAI model [73]. The large degree of incomplete switching observed in Microstructure-2 is primarily due to the insufficient load applied to trigger the switching. In case of varied loading with strain rate of $10^{-4}s^{-1}$, the coefficient of determination is similar to that for the constant loading as shown in Fig. 5c, and the plot suggests that the KAI theory is also reliable for the varied loading condition, but with $n > 5$. In Microstructure-2 and for strain rate of $10^{-6}s^{-1}$, the fitting has been good with $n > 3$. It was reported that ferroelastic domain switching under mechanical loading in PZT follows KAI dynamics, therefore these simulations are consistent with experiments [74]. However, we observe poor fitting in Fig. 5c in Microstructure-1 for strain rate of $10^{-6}s^{-1}$ suggesting that the dynamics of domain switching is complex and cannot be explained by the KAI theory alone.

In the present simulations, nucleation events rapidly saturate (in the constant loading condition) or compared to the total switching time, the duration of nucleation is negligible (in the varied loading condition). Therefore, the kinetics of domain switching is clearly dominated by domain wall propagation, and it is therefore category 2 of the KAI model [75]. This behavior is certainly inconsistent with NLS theory. This is most likely because of the fact that the nucleation events in the present simulations are few and it is restricted to c/a_1 domain walls only. In real polycrystalline materials far more nucleation sites are available with a wide range of nucleation barriers so that nucleation rate is significantly high to dominate over the propagation of domain wall. Furthermore, we observe in Fig. 4c and S1c that the domain propagation mostly proceeds in one major direction and less switching takes place in the other directions, and this explains why $n < 2$ as expected from the KAI dynamics. This is also consistent with the plots of velocity under constant loading in Fig. 6, where the domain wall velocity is mostly constant.

The KAI model is valid for the constant loading condition as it considers a constant domain wall velocity. Nevertheless, we have plotted Fig. 5c for the varied loading condition, and higher values of n are due to the time dependence of domain wall velocity. Higher values of n are frequently observed in non-isothermal Avrami kinetics [76]. In Fig. 7, we have plotted domain wall velocity along two directions at certain locations, and it suggests that the domain wall velocity is a complex nonlinear function of time. However, the time exponent gives the sense of average domain wall velocity in the whole volume which, however, cannot be established from Fig. 7. In general, we have observed that the kinetics of domain switching satisfactorily agree with the KAI model suggesting that the propagation of domain walls plays the dominant role determining the kinetics of domain switching.

3.3. Velocity of domain walls during switching

If the kinetics is dominated by propagation of domain walls, then the velocity of domain walls must be controlling the kinetics of domain switching. To evaluate the influence of domain wall velocity, we have chosen four locations: X_1 and X_2 in Microstructure-1 and Y_1 and Y_2 in

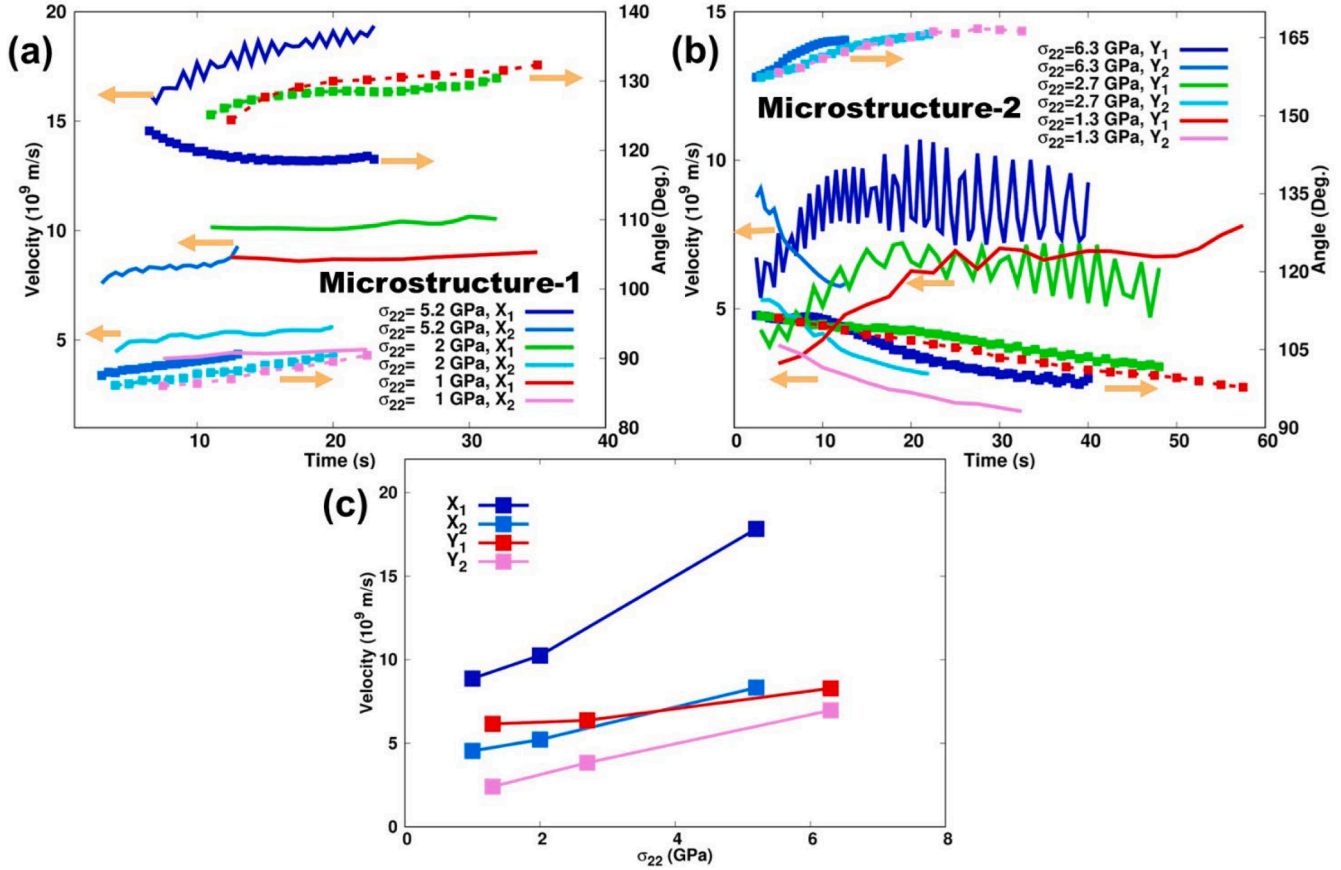

Fig. 6. The normal domain wall velocity (v_n) and angle (θ) that the normal to the domain wall makes with x_1 axis at X_1, X_2, Y_1 and Y_2 locations are plotted for (a) Microstructure-1 and (b) Microstructure-2 under constant loading. The solid lines represent the plot of velocity while the dashed lines with square datapoints represent the variation of angle with switching time. (c) The variation of the normal velocity with the applied load.

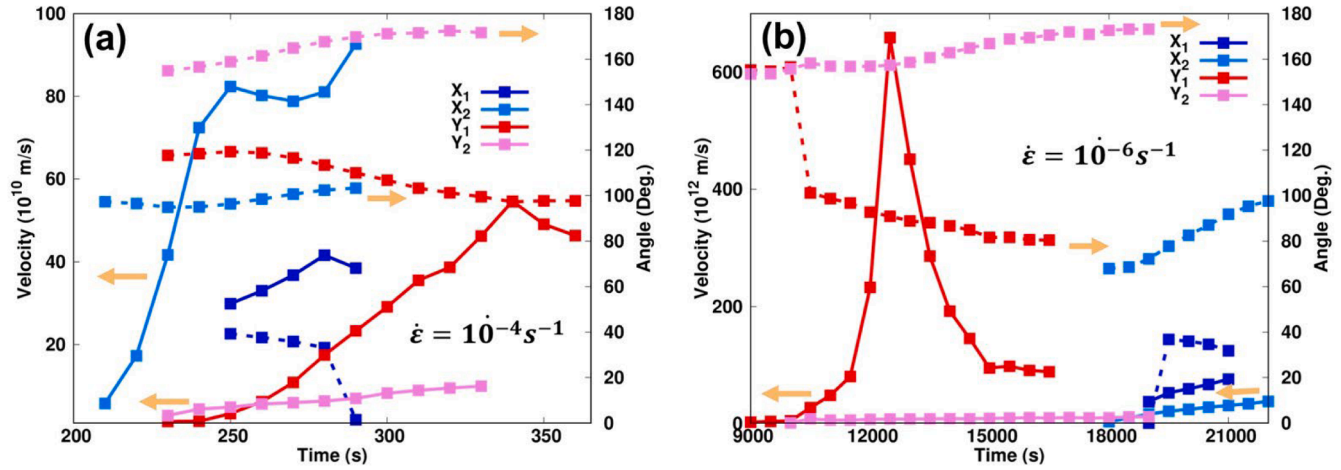

Fig. 7. The variation of the normal domain wall velocity (v_n) with time in the locations marked as X_1 and X_2 in Microstructure-1 and Y_1 and Y_2 in Microstructure-2 for strain rates of (a) $10^{-4}s^{-1}$ and (b) $10^{-6}s^{-1}$. The solid lines represent the plot of velocity while dashed lines represent the variation of angle (θ) with switching time.

Microstructure-2. We have calculated the normal velocity (v_n) of the domain walls along x_1 and x_2 axes and their inclination angle (θ) with x_1 axis by using Eq. (11) and Eq. (10), respectively, in these locations as shown in Fig. 4c, Fig. S1c, Fig. 8 and Fig. S4 by dashed yellow arrows. At X_1 location in Microstructure-1, a_1 domains switch into a_2 domains ($a_1 \rightarrow a_2$ switching), but at X_2 location in Microstructure-1 and at Y_1 and Y_2 locations in Microstructure-2 c domains switch into a_2 domains ($c \rightarrow a_2$ switching). In Microstructure-2, particularly in the case of varied loading, $a_1 \rightarrow a_2$ switching is however not observed, and $c \rightarrow a_2$ switching prevails, resulting in $c|a_2$ domain wall movement. In Fig. 6 (constant loading) and Fig. 7 (varied loading), we have plotted v_n and θ as a function of switching time. In Fig. 6, we observe that v_n does not appreciably vary with switching time, and the domain wall barely undergoes any rotation as θ remains almost steady at 90^o for X_2 and 125^o for X_1 locations. Similarly, in Microstructure-2 at Y_1 and Y_2 locations, θ is approximately 110^o and 160^o, respectively. In Fig. 6c, we have plotted

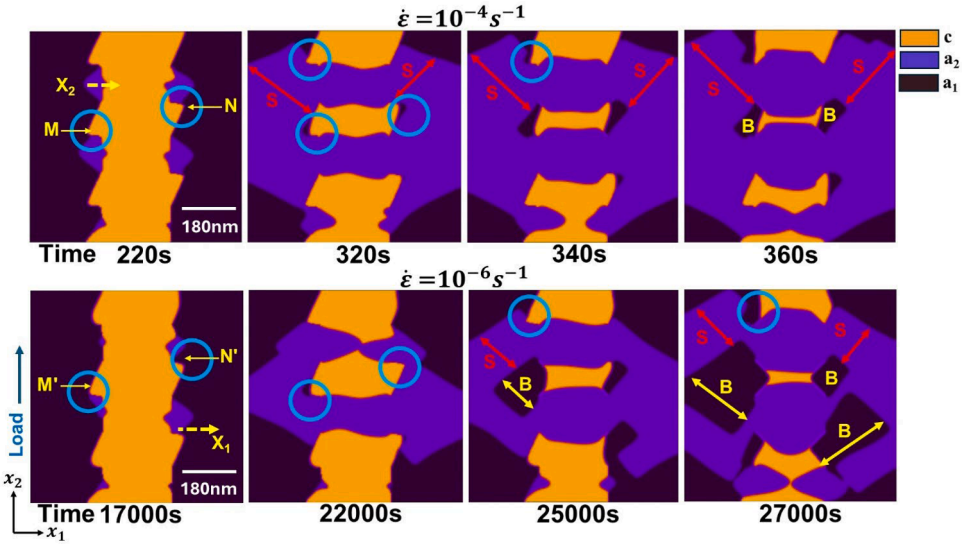

Fig. 8. The evolution of Microstructure-1 during tensile loading at strain rates of $10^{-4}s^{-1}$ (top row) and $10^{-6}s^{-1}$ (bottom row). In the region marked by cyan colored circle, sharp corners on $c|a_2$ domain wall nucleate the back-switched a_1 domains which are marked by "B". The region marked by "S" represents switched a_2 domains.

constant velocities as a function of applied stress. It should be mentioned that in the case of increasing velocities, an average velocity is considered. According to this plot, the normal domain wall velocity is almost linearly proportional to the applied stress. This linear relationship is consistent with the theory of diffusionless transformation, and a similar trend of constant velocity of domain wall under constant external stimulus was observed in other ferroic materials, such as $LiTaO_3$ [18,19,21]. In Fig. 6c, we also observe that at X_1 location, v_n is consistently larger than those at the other locations. This is due to the presence of a sharp corner at X_1 location where a higher level of accumulated stress results in a faster domain switching. This behavior is quite consistent with an experimental observation where the tip of a needle shaped domain was reported to have a velocity an order higher than that in the sidewise direction due to accumulation of higher stress at the sharp tip [37].

The plots of normal domain wall velocity (v_n) under varied loading in Fig. 7 are certainly not constant, except for the Y_1 location at the strain rate of $10^{-6}s^{-1}$, where the domain walls do not undergo any significant rotation. We observe that the velocity of $a_1|a_2$ domain wall consistently increases with time until it approaches the boundary of simulation domain when its inclination angle changes, as observed in Microstructure-1 for strain rate of $10^{-4}s^{-1}$(see Fig. 8). Similarly, $c|a_2$ domain walls are also observed to accelerate particularly along Y_1 under both strain rates, and the rapid acceleration here is also accompanied by the rotation of domain wall resulting in its alignment along x_2 axis. A large driving force originating from applied stress is responsible for such rapid acceleration. This behavior is expected as there is no opposing/pinning force present in the microstructure [26]. The rapid acceleration along Y_1 is eventually stopped by another $c|a_2$ domain wall approaching in the opposite direction, and due to the interaction with the other domain wall (see Fig. S2), the velocity decreases along Y_1. Apparently, there exists a critical distance between two domain walls above which they do not interact with each other, and under these circumstances, the domain wall accelerates. However, once the separation is less than the critical value, the velocity of domain walls reduces due to mutual interactions. In an experiment involving thin film of PZT, it was observed that domain walls separated by a distance of 2μm behave independent of each other, but for a separation <85 nm, they start to interact [20]. In some experiments, jerky' motion of domain wall has been observed due to pinning of domain wall and subsequently its release at higher strength of applied field [21–23,77]. Though jerky motion of domain wall is not observed in the present work, the opposing force on domain wall exerted by another domain wall is captured reasonably well in Fig. 7 and Fig. S2. The present simulation also suggests that an opposing force does not necessarily cause 'jerky' behavior of moving domain wall. Such a behavior possibly requires pinning by the presence of defects such as oxygen vacancies [78,79]. Even though the applied external load increases linearly with time, the acceleration of the domain walls as shown in Fig. 7 has not always been constant. Altogether, the simulations under both the loading conditions in both the microstructures have clearly demonstrated that the motion of domain wall is steady enough both in terms of its velocity and alignment that it dominates the kinetics of domain switching.

3.4. Mechanism of back-switching

According to the KAI model, the volume fraction of a_2 domains should vary continuously with time. But in Figs. 4a, S1a, 5a and b, we observe that the evolution of a_2 domains is not always smooth as expected from the KAI model. Using one dimensional form of discrete Ginzburg-Landau model with back-switching, Ishibashi reported a similar kinetics of domain switching [80]. The deviation from the smooth behavior is due to the formation of back-switching region. As shown in Fig. 4c and Fig. S1c for the constant loading condition and in Fig. 8 for the varied loading condition, despite the nucleation process which is followed by propagation of $a_1|a_2$ domain walls, some a_2 domains at $c|a_2$ domain wall switch back to a_1 domains. These back-switched $a_1$domains are marked in these figures, and we discuss the formation of these domains in the following.

Under the constant loading condition and after nucleation, the back-switched a_1 domains grow due to switching of $c \rightarrow a_1$ domains. This is primarily due to the fact that c domains are less stable than a_1 domains. We observe that after completion of $c \rightarrow a_1$ switching, the back-switched a_1 domains do not further switch into a_2 domains even if in the rest of the microstructure $c \rightarrow a_2$ and $a_1 \rightarrow a_2$ switching takes place. From the evolution of microstructures plotted in Figs. 4c, S1c, S2 and S3, we observe that the nucleation and growth of back-switched a_1 domains occur for all the applied loads in Microstructure-1, but back-switching is not observed for the loads of 1.3 and 2.7 GPa in Microstructure-2. Therefore, it appears that back-switching is activated at different levels of stress in different microstructures. Under varied loading in Microstructure-1 (Fig. 8), after nucleation at the same $c|a_2$ domain wall, the back-switched a_1 domains expand by $a_2 \rightarrow a_1$ even though a_2 is more stable than a_1 domains under σ_{22} tensile stress. We further notice in

Fig. 8 that back-switched a_1 domain ('the region marked by 'B') expands right behind the a_2 domain formed by $a_1 \rightarrow a_2$ switching (marked by 'S'). For the strain rate of $10^{-6}s^{-1}$, the back-switched region has a larger area compared to that for $10^{-4}s^{-1}$.

To understand the mechanism of formation of back-switched region, in Fig. 9, we plot the distribution of stresses σ_{11} and σ_{22} in Microstructure-1 at the strain rate of $10^{-6}s^{-1}$. We study the evolution of back-switched domains within two regions named M' (encircled by a black colored circle) and N' (encircled by a blue colored circle). In both regions, $c|a_2$ domain walls develop sharp corners. Similar sharp corners on $c|a_2$ domain walls are also observed in both microstructures under the constant loading condition in Fig. 4c and Fig. S1c, and we have marked all these corners with cyan colored circles in these figures. According to Fig. 9, in front of these corners, σ_{22} is compressive in both M' and N' regions which makes a_2 domains unstable. At the same time and in the same locations, tensile σ_{11} exists and it increases the stability of a_1 domain compared with a_2 domains, therefore, a_1 domain nucleates in front of the sharp corners on the $c|a_2$ domain walls. After nucleation of back-switched a_1 domain, propagating $a_1|a_2$ domain walls also develop sharp corners which again result in a combination of compressive σ_{22} and tensile σ_{11} that promotes further $a_2 \rightarrow a_1$ switching and expands back-switched a_1 domains. If a higher tensile stress is applied, the compressive σ_{22} in front of the sharp corner can be averted and the tendency of back-switching can be reduced which result in more switching into a_2 domains.

There is an interesting observation in Fig. S4 that Microstructure-2 under both strain rates does not show formation of any back-switched region. This is primarily because $c \rightarrow a_2$ switching takes place predominantly and $a_1 \rightarrow a_2$ switching is almost absent. Since c domains are not stable under the plane stress condition, the back-switching to c domains never take place. On the other hand, due to the absence of any sharp corners on the $c|a_2$ domain wall, nucleation of back-switched a_1 domains does not take place in the same way as observed in M' and N' in Fig. 9. As observed in Fig. 4a, Fig. S1a (for 6.3 GPa) and S3 under constant loading condition, and in Fig. 5a at strain rate of $10^{-4}s^{-1}$, the formation of small back-switched region does not cause any significant deviation of kinetics from the KAI model, as mentioned earlier in Section 3.2 that the coefficient of determinations have been at least 0.98 in these cases. However, in Microstructure-1 at the strain rate of $10^{-6}s^{-1}$, Fig. 8 shows that area of a_1 domains is significantly large, and this results in large deviation of switching kinetics from the KAI model as shown in Fig. 5b and c. Such an intriguing observation has significant implications in ferroelastic behavior of YSZ and its suitability for critical applications such as thermal barrier coating where ferroelastic domain-switching resists the propagation of crack [57,66] .

To assess the energetics of back-switching, we have calculated the elastic energy at a point in the region M' in Fig. 9 ahead of the corner, and the evolution of the elastic energy at that point (marked as a red spot) is plotted in Fig. 10. The variation of elastic energy can be observed to have three distinct stages. In stage 1, $a_1 \rightarrow a_2$ switching takes place in response to applied loading and the elastic energy decreases. In stage 2, $a_2 \rightarrow a_1$ back-switching takes place, and the elastic energy does not increase despite the application of tensile stress. Lowering of elastic energy is attributed to domain switching which absorbs the applied deformation energy [59]. However, at the end of stage 2 when back-switching saturates, the stress increases and the elastic energy also increases. In stage 3, due to further increase of tensile σ_{22}, a_2 domains again prevail and $a_1 \rightarrow a_2$ re-switching takes place which again decreases the elastic energy. The appearance of stage 3 is not observed for constant loading and at strain rate of $10^{-4}s^{-1}$. Apparently, stage 3 occurs only when the back-switched region becomes large enough by the movement of $a_1|a_2$ domain wall over a large distance driven by a favorable stress field. In contrast in small back-switched regions, $a_1|a_2$ domain wall does not have that opportunity.

It should be noted that the evolution of domains in the same Microstructure-1 described in section S2 of the supplementary material suggests that the tensile residual stress formed at the top surface of the topcoat does not alter the kinetics of a_2 domain evolution nor the normal

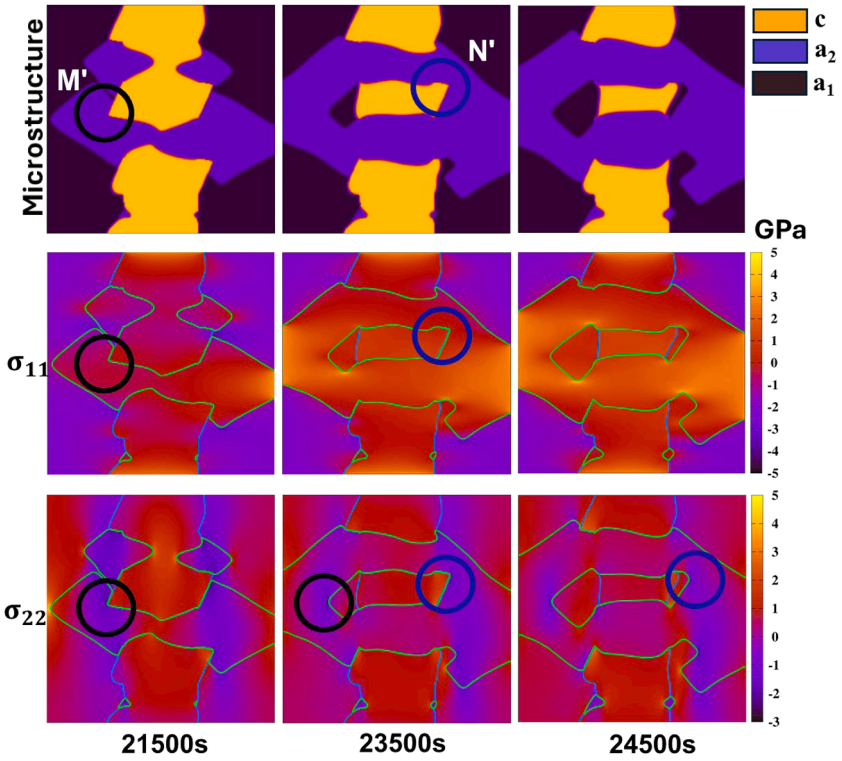

Fig. 9. The evolution of microstructure (top row), σ_{11} (middle row) and σ_{22} (bottom row) during formation of the back-switching region in Microstructure-1 under varied loading at strain rate of 10^{-6} s^{-1} .

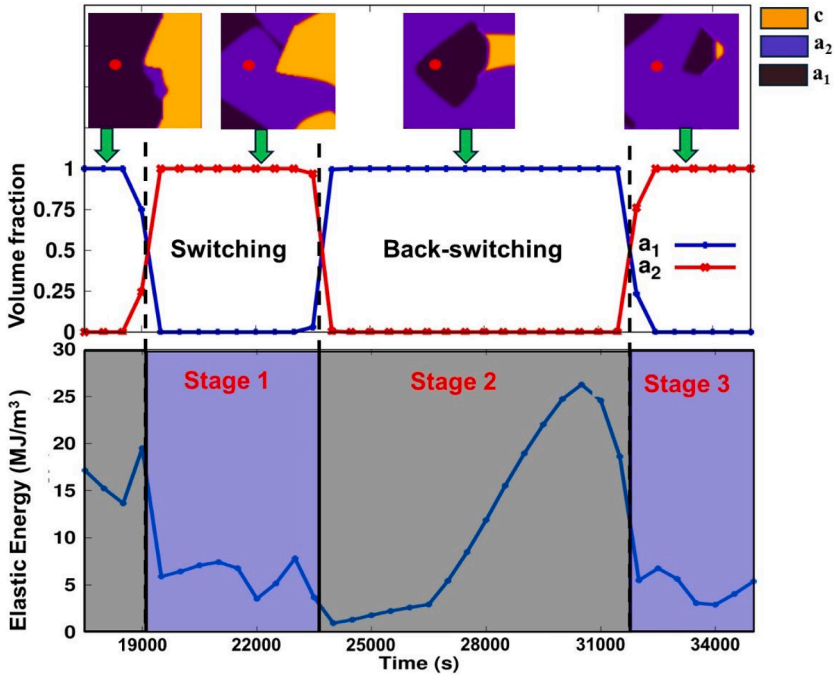

Fig. 10. The variation of elastic energy with time (bottom row) at a point marked as a red spot in the top row which depicts the evolution of microstructure. This point belongs to the region M' in Fig. 9 The corresponding variation of volume fractions of a_1 and a_2 domains are shown in the middle row.

domain wall velocity (as shown in Fig. S5a and Fig. S5b). The effect of compressive residual stress on the kinetics has also been minimal. In Fig. S5c, the formation of the same back-switching region suggests that this phenomenon, described in the context of kinetics of ferroelastic domain switching, is actually prevalent throughout the topcoat of t'-YSZ.

The occurrence of back-switched regions is expected to impact the behavior of ferroic materials. It is obvious that when the applied tensile stress is dropped to zero, the state of stress particularly at the corners of the back-switched regions can drive the $a_1|a_2$ domain walls depending on the elastic energy stored in these corners. In ferroelectric materials, which also exhibit ferroelasticity, the elastic energy stored at sharp corners of domain walls is expected to induce back-switching, resulting in a loss of retained polarization [38,39]. While back-switching may adversely affect the performance of ferroelectric materials, in purely ferroelastic materials, this phenomenon contributes to greater energy absorption. Consequently, fracture toughness can be further enhanced due to back-switching during stage 2 and subsequent re-switching in stage 3. This improvement can be highly advantageous for purely ferroelastic YSZ in critical applications, such as coatings for gas turbines [81] and pistons in combustion engines [82].

4. Conclusion

The present work for the first time describes the details of kinetics and the motion of domain wall during ferroelastic deformation in YSZ. The phase-field simulation results showed that the nucleation of domains does not significantly contribute to the kinetics of switching, and the ferroelastic domain switching primarily takes place by propagation of domain walls. Also, the domain switching kinetics mostly follows the KAI model. Under a constant loading condition, the domain wall velocity is constant, and it linearly varies with the applied stress, but under the varied loading conditions, the domain wall accelerates until it interacts with another domain wall or reaches the boundary. The present work suggests that a domain wall rarely rotates, and the steady velocity of the domain wall dominates the kinetics. The kinetics of domain switching reported in this work is largely consistent with theory [30,75] and experimental observations [22,31].

During reverse loading (or unloading), a sharp corner on a domain wall often results in a stress state so that the back-switching is promoted. The size of back-switched region depends on the loading conditions and the initial microstructure, and it plays an important role in incomplete domain switching as observed in experiments. The present work reports that the back-switching may be followed by another re-switching event which reduces the back-switched region in the microstructure. The complicated sequence of switching→back-switching→re-switching results in a significant deviation from KAI kinetics and a higher absorption of elastic energy. The complex sequence of switching and back-switching events, observed in this study for YSZ single crystals, will be investigated in future studies in other single and polycrystalline ferroelastic systems and by considering the influence of defects to draw more comprehensive conclusions on ferroelastic domain switching behaviors. Such studies are expected to provide more insights into detrimental back-switching behaviors in different applications, such as the loss of data in volatile memories [38,39] and performance degradation of sensors and actuators due to accumulation of irreversible ferroelastic strain [83,84].

Data availability

The datasets generated and/or analyzed in this study are available from the corresponding author on reasonable request.

CRediT authorship contribution statement

Avisor Bhattacharya: Writing – original draft, Visualization, Validation, Software, Methodology, Investigation, Formal analysis, Data curation, Conceptualization. **Mohsen Asle Zaeem:** Writing – review & editing, Supervision, Resources, Project administration, Methodology, Investigation, Funding acquisition, Formal analysis, Conceptualization.

Declaration of competing interest

The authors declare that they have no known competing financial interests or personal relationships that could have appeared to influence the work reported in this paper.

Acknowledgement

This work was supported by the U.S. Department of Energy, Office of Science, Basic Energy Sciences, under Award number DE-SC0019279. The authors are grateful for the for the supercomputing time allocation provided by the National Science Foundation's ACCESS (Advanced Cyberinfrastructure Coordination Ecosystem: Services & Support), Award No. TG-DMR140008.

Supplementary materials

Supplementary material associated with this article can be found, in the online version, at doi:10.1016/j.actamat.2024.120702.

References

[1] J.F. Scott, A review of ferroelectric switching, Ferroelectrics 503 (1) (2016) 117–132.
[2] J.F. Scott, C.A. Paz de Araujo, Ferroelectric memories, Science 246 (4936) (1989) 1400–1405.
[3] P. Muralt, Ferroelectric thin films for micro-sensors and actuators: a review, J. Micromech. Microeng. 10 (2) (2000) 136.
[4] D.R. Clarke, C.G. Levi, Materials design for the next generation thermal barrier coatings, Annu. Rev. Mater. Res. 33 (2003) 383–417, 332003.
[5] E.K.H. Salje, Ferroelastic materials, Annu. Rev. Mater. Res. 42 (2012) 265–283, 422012.
[6] S. Jesse, B.J. Rodriguez, S. Choudhury, A.P. Baddorf, I. Vrejoiu, D. Hesse, M. Alexe, E.A. Eliseev, A.N. Morozovska, J. Zhang, L.-Q. Chen, S.V. Kalinin, Direct imaging of the spatial and energy distribution of nucleation centres in ferroelectric materials, Nat. Mater. 7 (3) (2008) 209–215.
[7] A. Bhattacharya, M. Asle Zaeem, Mechanism of nucleation in ferroelastic domain switching, Scr. Mater. 252 (2024) 116273.
[8] R.E. García, B.D. Huey, J.E. Blendell, Virtual piezoforce microscopy of polycrystalline ferroelectric films, J. Appl. Phys. 100 (6) (2006) 064105-10.
[9] Y. Ivry, J.F. Scott, E.K.H. Salje, C. Durkan, Nucleation, growth, and control of ferroelectric-ferroelastic domains in thin polycrystalline films, Phys. Rev. B 86 (20) (2012) 205428.
[10] Y. Zhang, Y. Tan, D. Sando, L.-Q. Chen, N. Valanoor, Y. Zhu, M.-G. Han, Controlled nucleation and stabilization of ferroelectric domain wall patterns in epitaxial (110) bismuth ferrite heterostructures, Adv. Funct. Mater. 30 (48) (2020) 2003571.
[11] Y. Zhang, M.-G. Han, J.A. Garlow, Y. Tan, F. Xue, L.-Q. Chen, P. Munroe, N. Valanoor, Y. Zhu, Deterministic ferroelastic domain switching using ferroelectric bilayers, Nano Lett. 19 (8) (2019) 5319–5326.
[12] P. Gao, J. Britson, J.R. Jokisaari, C.T. Nelson, S.-H. Baek, Y. Wang, C.-B. Eom, L.-Q. Chen, X. Pan, Atomic-scale mechanisms of ferroelastic domain-wall-mediated ferroelectric switching, Nat. Commun. 4 (1) (2013) 2791.
[13] Author Index, in: J.W. Christian (Ed.), The Theory of Transformations in Metals and Alloys, Pergamon, Oxford, 2002, pp. A1–A16.
[14] W.J. Merz, Domain formation and domain wall motions in ferroelectric BaTiO3 single crystals, Phys. Rev. 95 (3) (1954) 690–698.
[15] P. Paruch, T. Giamarchi, T. Tybell, J.-M. Triscone, Nanoscale studies of domain wall motion in epitaxial ferroelectric thin films, J. Appl. Phys. 100 (5) (2006) 051608-10.
[16] T. Tybell, P. Paruch, T. Giamarchi, J.M. Triscone, Domain wall creep in epitaxial ferroelectric PbZr0.2Ti0.8O3 thin films, Phys. Rev. Lett. 89 (9) (2002) 097601.
[17] S.A. Kukushkin, M.A. Zakharov, Switching kinetics of ferroelastic ferroelectrics, Phys. Solid State 44 (12) (2002) 2298–2308.
[18] J.W. Christian, CHAPTER 11 - theory of thermally activated growth, in: J. W. Christian (Ed.), The Theory of Transformations in Metals and Alloys, Pergamon, Oxford, 2002, pp. 480–528.
[19] V. Gopalan, T.E. Mitchell, In situ video observation of 180° domain switching in LiTaO3 by electro-optic imaging microscopy, J. Appl. Phys. 85 (4) (1999) 2304–2311.
[20] L.J. McGilly, P. Yudin, L. Feigl, A.K. Tagantsev, N. Setter, Controlling domain wall motion in ferroelectric thin films, Nat. Nanotechnol. 10 (2) (2015) 145–150.
[21] V. Gopalan, Q.X. Jia, T.E. Mitchell, In situ video observation of 180° domain kinetics in congruent LiNbO3 crystals, Appl. Phys. Lett. 75 (16) (1999) 2482–2484.
[22] V.Y. Shur, E.V. Nikolaeva, E.I. Shishkin, V.L. Kozhevnikov, A.P. Chernykh, K. Terabe, K. Kitamura, Polarization reversal in congruent and stoichiometric lithium tantalate, Appl. Phys. Lett. 79 (19) (2001) 3146–3148.
[23] R.J. Harrison, E.K.H. Salje, The noise of the needle: avalanches of a single progressing needle domain in LaAlO3, Appl. Phys. Lett. 97 (2) (2010).
[24] Y. Kim, H. Han, W. Lee, S. Baik, D. Hesse, M. Alexe, Non-Kolmogorov–Avrami–Ishibashi switching dynamics in nanoscale ferroelectric capacitors, Nano Lett. 10 (4) (2010) 1266–1270.
[25] A. Gruverman, D. Wu, J.F. Scott, Piezoresponse force microscopy studies of switching behavior of ferroelectric capacitors on a 100-ns time scale, Phys. Rev. Lett. 100 (9) (2008) 097601.
[26] W.T. Lee, E.K.H. Salje, L. Goncalves-Ferreira, M. Daraktchiev, U. Bismayer, Intrinsic activation energy for twin-wall motion in the ferroelastic perovskite CaTiO3, Phys. Rev. B 73 (21) (2006) 214110.
[27] S.A. Kukushkin, M.A. Zakharov, Thermodynamics and kinetics of switching in ferroelastics-ferroelectrics the initial stage, Ferroelectrics 280 (1) (2002) 35–52.
[28] S.A. Kukushkin, A.V. Osipov, Thermodynamics and kinetics of switching effects in ferroelectrics, Phys. Rev. B 65 (17) (2002) 174101.
[29] A. Gruverman, B.J. Rodriguez, C. Dehoff, J.D. Waldrep, A.I. Kingon, R. J. Nemanich, J.S. Cross, Direct studies of domain switching dynamics in thin film ferroelectric capacitors, Appl. Phys. Lett. 87 (8) (2005) 082902-3.
[30] Y. Ishibashi, Theoretical aspects of polarization reversal in ferroelectrics, in: Proceedings of the [Proceedings] 1990 IEEE 7th International Symposium on Applications of Ferroelectrics, 1990, pp. 129–130.
[31] W. Li, M. Alexe, Investigation on switching kinetics in epitaxial Pb(Zr0.2Ti0.8)O3 ferroelectric thin films: role of the 90° domain walls, Appl. Phys. Lett. 91 (26) (2007) 262903-3.
[32] D. Pantel, Y.-H. Chu, L.W. Martin, R. Ramesh, D. Hesse, M. Alexe, Switching kinetics in epitaxial BiFeO3 thin films, J. Appl. Phys. 107 (8) (2010) 084111-4.
[33] J.Y. Jo, H.S. Han, J.G. Yoon, T.K. Song, S.H. Kim, T.W. Noh, Domain switching kinetics in disordered ferroelectric thin films, Phys. Rev. Lett. 99 (26) (2007) 267602.
[34] D. Kędzierski, E.V. Kirichenko, V.A. Stephanovich, On the theory of domain switching kinetics in ferroelectrics, Phys. Lett. A 375 (3) (2011) 685–688.
[35] P. Gao, C.T. Nelson, J.R. Jokisaari, Y. Zhang, S.-H. Baek, C.W. Bark, E. Wang, Y. Liu, J. Li, C.-B. Eom, X. Pan, Direct observations of retention failure in ferroelectric memories, Adv. Mater. 24 (8) (2012) 1106–1110.
[36] A. Gruverman, Recent advances in functional testing of ferroelectric nanostructures, Ferroelectrics 433 (1) (2012) 88–106.
[37] P. Gao, J. Britson, C.T. Nelson, J.R. Jokisaari, C. Duan, M. Trassin, S.-H. Baek, H. Guo, L. Li, Y. Wang, Y.-H. Chu, A.M. Minor, C.-B. Eom, R. Ramesh, L.-Q. Chen, X. Pan, Ferroelastic domain switching dynamics under electrical and mechanical excitations, Nat. Commun. 5 (1) (2014) 3801.
[38] I.G. Jenkins, T.K. Song, S. Madhukar, A.S. Prakash, S. Aggarwal, R. Ramesh, Dynamics of polarization loss in (Pb, La)(Zr, Ti)O3 thin film capacitors, Appl. Phys. Lett. 72 (25) (1998) 3300–3302.
[39] R.E. Jones, P.D. Maniar, R. Moazzami, P. Zurcher, J.Z. Witowski, Y.T. Lii, P. Chu, S. J. Gillespie, Ferroelectric non-volatile memories for low-voltage, low-power applications, Thin Solid Films 270 (1) (1995) 584–588.
[40] R.R. Mehta, B.D. Silverman, J.T. Jacobs, Depolarization fields in thin ferroelectric films, J. Appl. Phys. 44 (8) (1973) 3379–3385.
[41] X.J. Lou, Polarization retention on short, intermediate, and long time scales in ferroelectric thin films, J. Appl. Phys. 105 (9) (2009).
[42] B.S. Kang, J.-G. Yoon, T.W. Noh, T.K. Song, S. Seo, Y.K. Lee, J.K. Lee, Polarization dynamics and retention loss in fatigued PbZr0.4Ti0.6O3 ferroelectric capacitors, Appl. Phys. Lett. 82 (2) (2003) 248–250.
[43] A. Gruverman, M. Tanaka, Polarization retention in SrBi2Ta2O9 thin films investigated at nanoscale, J. Appl. Phys. 89 (3) (2001) 1836–1843.
[44] A. Gruverman, H. Tokumoto, A.S. Prakash, S. Aggarwal, B. Yang, M. Wuttig, R. Ramesh, O. Auciello, T. Venkatesan, Nanoscale imaging of domain dynamics and retention in ferroelectric thin films, Appl. Phys. Lett. 71 (24) (1997) 3492–3494.
[45] A. Morelli, S. Venkatesan, G. Palasantzas, B.J. Kooi, J.T.M. De Hosson, Polarization retention loss in PbTiO3 ferroelectric films due to leakage currents, J. Appl. Phys. 102 (8) (2007) 084103-6.
[46] M. Mamivand, M. Asle Zaeem, H. El Kadiri, L.-Q. Chen, Phase field modeling of the tetragonal-to-monoclinic phase transformation in zirconia, Acta Mater. 61 (14) (2013) 5223–5235.
[47] B. Xu, G. Kang, Phase field simulation on the super-elasticity, elastocaloric and shape memory effect of geometrically graded nano-polycrystalline NiTi shape memory alloys, Int. J. Mech. Sci. 201 (2021) 106462.
[48] A. Lotfolahpour, W. Huber, M.Asle Zaeem, A phase-field model for interactive evolution of phase transformation and cracking in superelastic shape memory ceramics, Comput. Mater. Sci. 216 (2023) 111844.
[49] S. Choudhury, Y.L. Li, C.E. Krill, L.Q. Chen, Phase-field simulation of polarization switching and domain evolution in ferroelectric polycrystals, Acta Mater. 53 (20) (2005) 5313–5321.
[50] S. Choudhury, Y.L. Li, C. Krill, L.Q. Chen, Effect of grain orientation and grain size on ferroelectric domain switching and evolution: phase field simulations, Acta Mater. 55 (4) (2007) 1415–1426.
[51] S. Choudhury, J.X. Zhang, Y.L. Li, L.Q. Chen, Q.X. Jia, S.V. Kalinin, Effect of ferroelastic twin walls on local polarization switching: phase-field modeling, Appl. Phys. Lett. 93 (16) (2008).
[52] J.X. Zhang, L.Q. Chen, Phase-field model for ferromagnetic shape-memory alloys, Philos. Mag. Lett. 85 (10) (2005) 533–541.
[53] Q. Peng, Y.J. He, Z. Moumni, A phase-field model on the hysteretic magneto-mechanical behaviors of ferromagnetic shape memory alloy, Acta Mater. 88 (2015) 13–24.
[54] P.P. Wu, X.Q. Ma, J.X. Zhang, L.Q. Chen, Phase-field simulations of magnetic field-induced strain in Ni2MnGa ferromagnetic shape memory alloy, Philos. Mag. 91 (16) (2011) 2102–2116.
[55] Y.L. Li, S.Y. Hu, Z.K. Liu, L.Q. Chen, Effect of substrate constraint on the stability and evolution of ferroelectric domain structures in thin films, Acta Mater. 50 (2) (2002) 395–411.
[56] Z.P. Pi, F. Zhang, J.B. Chen, W. Zhu, L. Yang, Y.C. Zhou, Multiphase field theory for ferroelastic domain switching with an application to tetragonal zirconia, Comput. Mater. Sci. 170 (2019) 109165.
[57] Y. Sun, J. Luo, J. Zhu, Ferroelastic toughening of single crystalline yttria-stabilized t' zirconia: a phase field study, Eng. Fract. Mech. 233 (2020) 107077.

[58] J. Li, Q. Zhou, L. Yang, Y. Zhou, J. Zhao, J. Huang, Y. Wei, Ferroelastic deformation mechanism and mechanical properties of [001]-oriented YSZ film by indentation, J. Alloy. Compd. 889 (2021) 161557.
[59] A. Bhattacharya, M.Asle Zaeem, A phase-field model for study of ferroelastic deformation behavior in yttria stabilized zirconia, Acta Mater. 276 (2024) 120039.
[60] K.M. Prettyman, J.F. Jue, A.V. Virkar, C.R. Hubbard, O.B. Cavin, M.K. Ferber, Hysteresity effects in 3 mol% yttria-doped zirconia (t'-phase), J. Mater. Sci. 27 (15) (1992) 4167–4174.
[61] U. Messerschmidt, D. Baither, B. Baufeld, M. Bartsch, Plastic deformation of zirconia single crystals: a review, Mater. Sci. Eng. A 233 (1) (1997) 61–74.
[62] C.-J. Chan, F.F. Lange, M. Rühle, J.-F. Jue, A.V. Virkar, Ferroelastic domain switching in tetragonal zirconia single crystals—microstructural aspects, J. Am. Ceram. Soc. 74 (4) (1991) 807–813.
[63] D. Baither, M. Bartsch, B. Baufeld, A. Tikhonovsky, A. Foitzik, M. Rühle, U. Messerschmidt, Ferroelastic and plastic deformation of t′-zirconia single crystals, J. Am. Ceram. Soc. 84 (8) (2001) 1755–1762.
[64] K. Noguchi, M. Fujita, T. Masaki, M. Mizushina, Tensile strength of yttria-stabilized tetragonal zirconia polycrystals, J. Am. Ceram. Soc. 72 (7) (1989) 1305–1307.
[65] M. Muramoto, J. Tatami, M. Iijima, K. Matsui, T. Yahagi, T. Takahashi, H. Nakano, T. Ohji, Deformation behavior and bending strength of single crystal 8 mol% yttria-stabilized zirconia at microscopic scale, J. Eur. Ceram. Soc. 44 (2) (2024) 1061–1069.
[66] A.V. Virkar, R.L.K. Matsumoto, Ferroelastic domain switching as a toughening mechanism in tetragonal zirconia, J. Am. Ceram. Soc. 69 (10) (1986) 226. C-224-C.
[67] H. Masuda, K. Morita, M. Watanabe, T. Hara, H. Yoshida, T. Ohmura, Ferroelastic and plastic behaviors in pseudo-single crystal micropillars of nontransformable tetragonal zirconia, Acta Mater. 203 (2021) 116471.
[68] M. Li, B. Wang, H.-J. Liu, Y.-L. Huang, J. Zhang, X. Ma, K. Liu, D. Yu, Y.-H. Chu, L.-Q. Chen, P. Gao, Direct observation of weakened interface clamping effect enabled ferroelastic domain switching, Acta Mater. 171 (2019) 184–189.
[69] V. Teixeira, M. Andritschky, W. Fischer, H.P. Buchkremer, D. Stöver, Analysis of residual stresses in thermal barrier coatings, J. Mater. Process. Technol. 92-93 (1999) 209–216.
[70] B. Baufeld, D. Baither, U. Messerschmidt, M. Bartsch, A.H. Foitzik, M. Rühle, Ferroelasticity of t'-Zirconia: II, in situ straining in a high-voltage electron microscope, J. Am. Ceram. Soc. 80 (7) (1997) 1699–1705.
[71] B. Wang, L.-Q. Chen, Theory of strain phase equilibria and diagrams, Acta Mater. 274 (2024) 120025.
[72] R.C. Miller, G. Weinreich, Mechanism for the sidewise motion of 180° domain walls in barium titanate, Phys. Rev. 117 (6) (1960) 1460–1466.
[73] J. Kakalios, R.A. Street, W.B. Jackson, Stretched-exponential relaxation arising from dispersive diffusion of hydrogen in amorphous silicon, Phys. Rev. Lett. 59 (9) (1987) 1037–1040.
[74] Q. Li, B. Wang, Q. He, P. Yu, L.-Q. Chen, S.V. Kalinin, J.-F. Li, Ferroelastic nanodomain-mediated mechanical switching of ferroelectricity in thick epitaxial films, Nano Lett. 21 (1) (2021) 445–452.
[75] Y. Ishibashi, Y. Takagi, Note on ferroelectric domain switching, J. Phys. Soc. Jpn. 31 (2) (1971) 506–510.
[76] L.V. Meisel, P.J. Cote, Non-isothermal transformation kinetics: application to metastable phases, Acta Metall. 31 (7) (1983) 1053–1059.
[77] S. Puchberger, V. Soprunyuk, W. Schranz, A. Tröster, K. Roleder, A. Majchrowski, M.A. Carpenter, E.K.H. Salje, The noise of many needles: jerky domain wall propagation in PbZrO3 and LaAlO3, APL Mater. 5 (4) (2017) 046102-7.
[78] C. Wang, Q.F. Fang, Y. Shi, Z.G. Zhu, Internal friction study on oxygen vacancies and domain walls in Pb(Zr, Ti)O3 ceramics, Mater. Res. Bull. 36 (15) (2001) 2657–2665.
[79] R.J. Harrison, S.A.T. Redfern, J. Street, The effect of transformation twins on the seismic-frequency mechanical properties of polycrystalline Ca1−xSrxTiO3 perovskite, Am. Mineral. 88 (4) (2003) 574–582.
[80] Y. Ishibashi, A model of polarization reversal in ferroelectrics, J. Phys. Soc. Jpn. 59 (11) (1990) 4148–4154.
[81] M.A. Alvin, K. Klotz, B. McMordie, D. Zhu, B. Gleeson, B. Warnes, Extreme temperature coatings for future gas turbine engines, J. Eng. Gas. Turbine Power. 136 (11) (2014).
[82] G.X. Lu, L.J. Hao, C. Liu, F.X. Ye, Thermal analysis and failure behaviour of YSZ thermal barrier coatings on low heat rejection diesel engine piston, Mater. Sci. Technol. 30 (11) (2014) 1273–1281.
[83] S. Pojprapai, Z. Luo, B. Clausen, S.C. Vogel, D.W. Brown, J. Russel, M. Hoffman, Dynamic processes of domain switching in lead zirconate titanate under cyclic mechanical loading by in situ neutron diffraction, Acta Mater. 58 (6) (2010) 1897–1908.
[84] S. Pojprapai, J.L. Jones, A.J. Studer, J. Russell, N. Valanoor, M. Hoffman, Ferroelastic domain switching fatigue in lead zirconate titanate ceramics, Acta Mater. 56 (7) (2008) 1577–1587.